Nitric Oxide 86 (2019) 38–47

Contents lists available at ScienceDirect

Nitric Oxide

journal homepage: www.elsevier.com/locate/yniox

Cytotoxicity, cellular uptake, and subcellular localization of a nitrogen oxide and aminopropyl-β-lactose derivative ruthenium complex used as nitric oxide delivery agent

Joicy Santamalvina dos Santos[a,b], Loyanne C. Ramos[a], Lucimara P. Ferreira[c], Vanessa Leira Campo[a,d], Lucas C.D. de Rezende[a], Flávio da Silva Emery[a], Roberto Santana da Silva[a,*]

[a] Departamento de Física e Química, Faculdade de Ciências Farmacêuticas de Ribeirão Preto, Universidade de São Paulo, Av. Prof. Zeferino Vaz s/n, CEP, 14040-903, Ribeirão Preto, SP, Brazil
[b] Departamento de Química Geral e Inorgânica, Instituto de Química, Universidade Federal da Bahia, Rua Barão de Geremoabo, 147, Campus Universitário de Ondina, C. E.P. 40.170-115, Salvador, BA, Brazil
[c] Departamento de Física, Faculdade de Filosofia, Ciências e Letras de Ribeirão Preto, Universidade de São Paulo, Av. Bandeirantes, 3900, CEP, 14040-901, Ribeirão Preto, SP, Brazil
[d] Barão de Mauá University Centre, 423 Ramos de Azevedo Street, Jardim Paulista, CEP 14090-180, Ribeirão Preto, SP, Brazil

ARTICLE INFO

Keywords:
Nitric oxide donor agents
Ruthenium-nitrite complex
Cytotoxicity
Metal-based drugs

ABSTRACT

This work investigates how the luminescent ruthenium-nitrite complexes *cis*-[Ru(py-bodipy)(dcbpy)$_2$(NO$_2$)](PF$_6$) **(I)** and *cis*-[Ru(py-bodipy)(dcbpy-aminopropyl-β-lactose)$_2$(NO$_2$)](PF$_6$) **(II)** behave toward the melanoma cancer cell line B16F10. The chemical structure and purity of the synthesized complexes were analyzed by UV-Visible and FTIR spectroscopy, MALDI, HPLC, and ^{1}H NMR. Spectrofluorescence helped to determine the fluorescence quantum yields and lifetimes of each of these complexes. *In vitro* MTT cell viability assay on B16F10 cancer cells revealed that the complexes possibly have a tumoricidal role. The metal-nitrite complexes evidenced the dichotomous NO nature: at high concentration, NO exerted a tumoricidal effect, whereas cancer cells grew at low NO concentration. Flow cytometry or fluorescence microscopy aided cellular uptake calculation. Cell staining followed by fluorescence microscopy associated with organelle markers such as DAPI and Rhodamine 123 detected preferential intracellular localization of the ruthenium-nitrite py-bodipy and aminopropyl lactose derivative ruthenium complex in mitochondria. Thus, the cytotoxicity of compounds **(I)** and **(II)** against B16F10 cancer cell line show concentration-dependent results. The present studies suggest that nitric oxide ruthenium derivative compounds could be new potential chemotherapeutic agents against cytotoxic cells.

1. Introduction

The use of coordination compounds as drugs or pro-drugs has been proposed due to the great versatility of the metal ion oxidation state depending on the ligand(s) [1–4]. Among several biological activities, the antitumor properties of metal-based compounds have been extensively studied since cisplatin was discovered as a potent chemotherapeutic agent [5–8]. On the fundamentals of cancer chemotherapy metal complexes have essentially been developed on the basis of hydrolysis, protein binding, membrane transportation, and interaction with the molecular target [9–11]. However, many studies have failed to describe how cytotoxicity is related to the cellular uptake and subcellular localization of these compounds in cancer cell lines, which has prevented the cell death mechanism from being fully elucidated. Labeled fluorescent ligand binding to the coordination metal may give information about the biological target of metal-based drugs and their cellular uptake. In this context, boron-dipyrromethene compounds, commonly known as bodipy, may represent a promising class of fluorophores that can be applied as fluorescent dyes. Bodipy generally have high molar extinction coefficient in the visible region, high lipophilicity, and high fluorescence quantum yield, and these ligands are resistant to photobleaching and reasonably stable in physiological conditions [12–14]. These properties make bodipy compounds a useful tool to label compounds with relevant biological activity and provide the basis for direct binding assays. One possibility would be to obtain compounds by conjugating bodipy and ruthenium complex derivatives

* Corresponding author.
E-mail address: silva@usp.br (R. Santana da Silva).

https://doi.org/10.1016/j.niox.2019.02.005
Received 23 October 2018; Received in revised form 15 December 2018; Accepted 13 February 2019
Available online 19 February 2019
1089-8603/

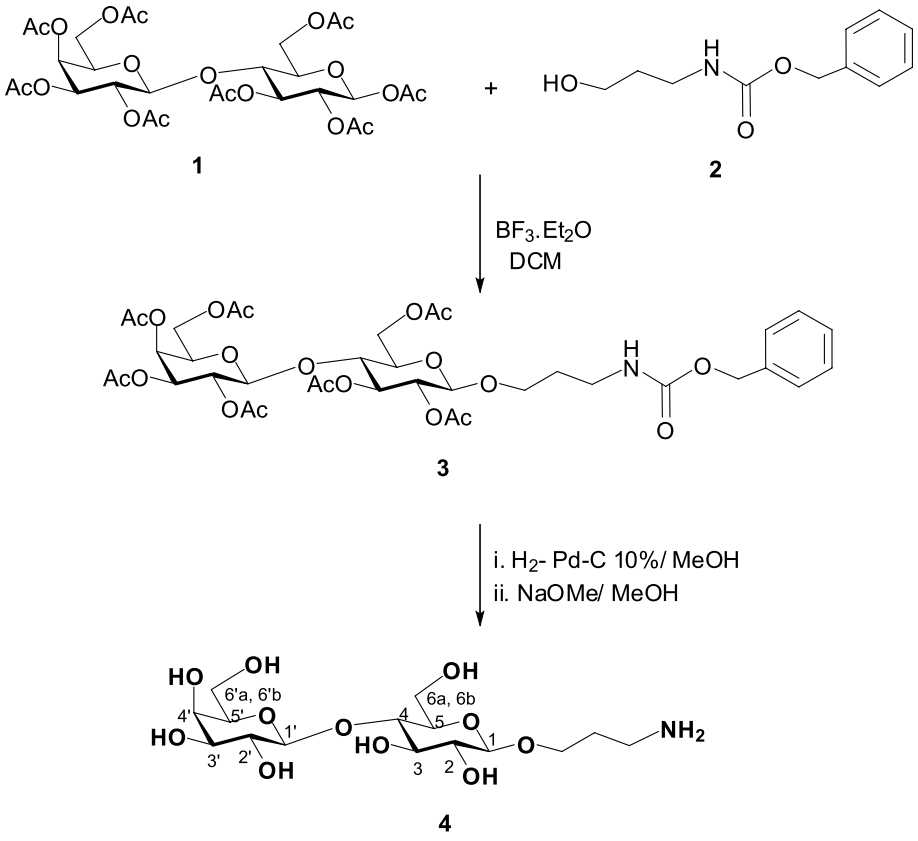

Scheme 1. Route for the synthesis of aminopropyl-β-lactose.

bearing nitrogen oxide (NO), giving rise to complexes that could act as NO delivery agents. NO participates in various regulatory functions, from cardiovascular system regulation to neural function modulation [15–18]. In addition, researchers have studied NO as an anti-cancer agent because it can exert tumoricidal effects or induce tumor growth depending on concentration, timing, and location [15–18]. In recent years, NO-derivative ruthenium compounds have been extensively investigated as NO delivery agents by light irradiation [19–21], oxygen transfer reaction [22,23], or reduction process [24,25]. In biological tests, these properties have been explored in vasorelaxation [26–28] and Chagas disease research [29,30]; more recently, they have been tested in cytotoxicity assays [31–34]. In this way, the design of nitric oxide derivative ruthenium complexes may act as site-directed delivery of NO into cancer cells, which provoke molecule changes triggering particular reactions [35]. Genotoxic effects occasioned by NO could be associated, for example, to the formation of nitrite and nitrate, S-nitroso-thiols or peroxynitrate, which are involved in DNA damage [35,36]. Based on this, several papers have been published and describing the processes related to the biochemical pathway of NO including cytotoxicity against cancer cells [15,16,18,27,37]. Fundamental understanding of NO-mediated cytotoxicity could lead to major advances in cancer drug development. In that case, the controlled NO release by ruthenium complexes activated chemically or photochemically may serve as prototype of metallotherapeutic drugs [17,19–21,24–26,28–32]. Despite the successful use of ruthenium species in biological assays, little information regarding its subcellular localization exists. In this scenario, biomarkers could help to predict the clinical outcome of these species.

Here, we designed a long-life highly luminescent ruthenium (II)-nitrite complexes, *cis*-[Ru(py-bodipy)(dcbpy)$_2$(NO$_2$)](PF$_6$) and *cis*-[Ru(py-bodipy)(dcbpy-aminopropyl-β-lactose)$_2$(NO$_2$)](PF$_6$) named here as **(I)** and **(II)** respectively, for application in cancer imaging and treatment. The carbohydrate moiety allows rapid cellular uptake as judge by flux cytometry assays. Cytotoxicity effects of the ruthenium complexes against B16F10 cells allows to understand NO dichotomy with cell viability decrease about 80% when we have used 150 μM. It was attributed to subcellular localization of this complex mainly centered on mitochondria.

2. Experimental

2.1. Synthesis of ligands

All the reagents were commercially available and had analytical grade purity unless otherwise stated. Reactions were monitored by thin-layer chromatography (TLC) on 0.25-nm pre-coated silica gel plates (Whatman, AL SIL G/UV, aluminum backing) with the indicated eluents. The tested compounds were visualized under UV light (254 nm) and/or dipping in ethanol/sulfuric acid (95:5, v/v), followed by heating of the plate for 2 min. Column chromatography was performed on silica gel 60 (Fluorochem, 35–70 mesh) or on a Biotage Horizon High-Performance FLASH Chromatography system by using 12-mm or 25-mm flash cartridges and the indicated eluents. Nuclear magnetic resonance spectra were recorded on Bruker Advance DRX 300 (300 MHz), DPX 400 (400 MHz), or DPX 500 (500 MHz) spectrometers. The chemical shifts (δ) are given in parts per million downfield from tetramethylsilane.

4,4′-dimethyl-2,2′-bypiridine, provided by Aldrich, was oxidized to 4,4′- dicarboxy-2,2′- bipyridine (dcbpy) based on a procedure adapted from the literature [38]; the yield was 96%. HRMS-ESI: $[M + H]^+$ calculated for $C_{12}H_9N_2O_4$ = 245.0560, found = 245.0561; FTIR (ν, cm^{-1}): 2450, 1720, 1890, 1285. The fluorescent ligand py-bodipy (4,4-difluoro-4-bora-3a, 4a-diaza-s-indacene) was synthesized from 4-pyridinocarboxyaldehyde (Aldrich), dimethyl pyrrole (Acros), and BF_3OEt_2, in dichloromethane and under magnetic stirring, as reported elsewhere [39]. The oily residue was purified by flash column chromatography (230–400 mesh, hexane/ethyl acetate/TEA 75:23:2), to give the product in 11% yield. ^{1}H NMR (500 MHz, $CDCl_3$) δ_H: 8.78 (d,

J = 5.3 Hz, 1H); 7.30 (d, J = 5.3 Hz, 1H); 6.00 (s, 1H); 2.55 (s, 3H); 1.40 (s, 3H). ^{13}C NMR (125 MHz, $CDCl_3$) δ_C: 156.59, 150.70, 150.04, 143.78, 142.77, 137.71, 130.44, 123.45, 121.93, 113.83, 77.16, 14.77, 14.75. HRMS-ESI: $[M + H]^+$ calculated for $C_{18}H_{19}BF_2N_3$ = 326.1714, found = 326.1643. FTIR (ν, cm^{-1}): 2918, 1654, 1508, 1466, 1410, 1306, 1156, 1120, 1076, 980, 812, 720.

Aminopropyl-β-lactose was prepared by following a procedure adapted from the literature [40], in two steps (Scheme 1): (i) glycosylation reaction between β-lactose (**1**) and benzyl 3-hydroxypropyl-carbamate (**2**), followed by (ii) benzyloxy carbonyl (Cbz) group cleavage through hydrogenolysis and acetyl group removal. β-D-lactose (**1**) (Acros Organics) was previously acetylated by reaction with acetic anhydride and I_2, which was followed by column chromatography purification (ethyl acetate/hexane 1:1 v/v). For the subsequent glycosylation reaction, acetylated β-D-lactose (1 g, 1.47 mM) was added to **2** (308 mg, 1.47 mM) under nitrogen atmosphere; dichloromethane and $BF_3.Et_2O$ (1 mL, 8.1 mM) were used as solvent and catalyst, respectively. The reaction mixture was magnetically stirred at room temperature for 7 h, and the product (**3**) was purified by flash chromatography (Biotage) (ethyl acetate/hexane, gradient method, 0–100% ethyl acetate), to give the product in 61% yield.

For the hydrogenolysis reaction, compound **3** (412.8 mg, 0.49 mM) was dissolved in a mixture of methanol (3 mL) and acetic acid (300 μL) and treated with Pd-C 10% (160 mg). The obtained mixture was stirred under H_2 atmosphere for 12 h, filtered through celite, and purified by flash chromatography (CH_2Cl_2/CH_3OH 8:2), affording the product in 36% yield. The final product **4** was achieved by deacetylation with 1 M sodium methoxide in methanol (pH 10). The mixture was stirred at room temperature for 5 h, neutralized with ion exchange resin (Dowex 50WX8-200 H^+), filtered, and concentrated under reduced pressure, which furnished product **4** in 71% yield. This product was characterized by ^{1}H NMR. δ_H ($CDCl_3$, 500 MHz) 4.51 (1H, d, J = 8.0 Hz, H-1); 4.29 (1H, d, J = 7.7 Hz, H-1′); 3.81 (1H, t, J = 10.4 Hz, H-3); 3.77 (1H, d, J = 3.1 Hz, H-4′); 3.73-3.37 (13H, H-3′, H-2, H-2′, H-5, H-5′, H-4, 2x CH_2, H-6a, H-6b, H-6′a, H-6′b); 3.13 (2H, t, J = 8.3 Hz, CH_2 NH_2).

2.2. Synthesis of the ruthenium complexes

$RuCl_3.3H_2O$ was purchased from Aldrich Chemicals and used as supplied. Acetonitrile from J. T. Baker, acetonitrile from Mallinckrodt, and methanol from Merck were employed. Double-distilled water was employed in all the experiments. All the preparations were carried out under argon atmosphere and protected from light.

The complex *cis*-$[RuCl_2(dcbpy)_2].2H_2O$ was prepared as described by Dwyer et al. [41]. The complex salt *cis*-$[Ru(NO_2)(dcbpy)_2(NO)](PF_6)_2$ was obtained as reported by Meyer et al. [42] and elsewhere [43]. The typical yield was 93%. Elemental analysis: Found: C, 30.75; H, 1.74; N, 8.69%. $RuC_{24}N_6H_{16}O_{11}P_2F_{12}$ requires C, 30.17; H, 1.69; N, 8.80%. Complex **(I)** was synthesized by subjecting 45 mg of *cis*-$[Ru(NO_2)(dcbpy)_2(NO)](PF_6)_2$, dissolved in acetone, to reflux at 70 °C and under magnetic stirring, to which 3 mg of NaN_3 previously dissolved in 3 mL of methanol was added dropwise. Then, 62 mg of the ligand py-bodipy was added to the reaction, which was monitored by thin layer chromatography ($CH_3OH/CH_2Cl_2/H_2O$ 10:10:1). After 16 h, the reaction was cooled, and the reaction flask was left at 10 °C overnight, to give a brown precipitate. The complex was filtered and washed with dichloromethane, and the final yield was 58%. Elemental analysis: Found: C, 46.07; H, 3.03; N, 10.26%. $RuC_{42}N_8H_{34}O_{10}BPF_8$ requires C, 45.63; H, 3.10; N, 10.13%.

The aminopropyl-β-lactose coupling reaction with **(I)** consisted in adding 10 mg of **(I)**, 13 mg of H-hydroxysuccinimide (NHS, Aldrich), and 13 mg of N,N′-bicyclo-hexyl carbodiimide (DCC) to a round-bottom flask containing dimethylformamide at room temperature and under magnetic stirring. Aminopropyl-β-lactose (15 mg) was added after 6 h of reaction. After the reaction was complete (48 h), the solvent was vacuum evaporated, and acetone was added. The ruthenium complex was precipitated after addition of petroleum ether and was analyzed by ^{1}H NMR, mass spectrometry, and HPLC to confirm its purity. ^{1}H NMR. δ_H (D_2O, 500 MHz) 4.325 (1H, d, J = 7.5 Hz, H-1); 3.85-3.33 (13H, H-3′, H-2, H-2′, H-5, H-5′, H-4, 2x CH_2, H-6a, H-6b, H-6′a, H-6′b); 3.15 (2H, t, J = 8.3 Hz, CH_2 NH_2).

2.3. Characterization of ligands and ruthenium complexes

The pH measurements were performed using a DM 20 pH meter (Digimed). UV/Vis spectra were recorded on an Agilent 8453 UV-visible device. FTIR spectra were registered on a Shimadzu IR-Prestige 21 system spectrometer; solid samples pressed in KBr pellets or in CH_2Cl_2 solution were used, and a SiO_2 window was employed. ^{1}H NMR spectra were acquired on a Bruker DRX 500-MHz from Bruker Daltonics. Fluorescence spectra were obtained on a Shimadzu RF5301PC spectrofluorimeter equipped with a xenon arc lamp as the light source; the excitation wavelength (λ_{exc}) was 470 nm. Molar extinction coefficients were calculated in ethanol or water. Quantum yields were obtained by a comparative method [44]; fluorescein in 0.1 M NaOH in water was used as standard (ϕ = 0.91, λ_{exc} = 470 nm) for the ligand py-bodipy, and *tris*-(bipyridine)ruthenium(II) chloride (Sigma) in H_2O was employed as standard (ϕ = 0.086, λ_{exc} = 485 nm) for the complexes [45]. Emission spectra of five samples of each fluorophore (absorbance between 0.1 and 0.001 at the excitation wavelength of 470 nm) were recorded. Results were plotted as the integrated fluorescence intensity vs absorbance, which provided the curve slope. A curve was constructed for each tested compound and the standards. The quantum yield of the tested compounds (ϕ_x) was calculated by using equation (1), where ϕ_{st} is the quantum yield of the standard, m_x and m_{st} are the slopes for the test compound and the standard compound, respectively, and η_x and η_{st} are solvent refractive indexes.

$$\phi_x = \phi_{st}\left[\frac{m_x}{m_{st}}\right]\left[\frac{n_x}{n_{st}}\right] \quad (1)$$

HPLC analyses were performed on a Shimadzu liquid chromatograph equipped with two LC-20AT solvent pumps, an SPD-M20A VP spectrophotometric detector (λ = 230 nm) coupled to a CBM-20A system controller, and an injector with a 20-μL loop. The device was connected to a diode array spectrophotometer. The ruthenium complexes were separated on a C18 Zorbax column (Agilient) with 5-μm particle size (250 × 4.6 mm). The analytical column was protected by a C18 Zorbax guard column (4 × 4 mm), which was also purchased from Agilient. The mobile phase consisted of an isocratic flow of Milli-Q water/CH_3OH 80:20 (v/v) at a flow rate of 1 mL min^{-1}. The total elution time was 30 min. The mobile phase was purged with helium. Samples were solubilized in 500 μL of mobile phase. Matrix assisted laser desorption ionization (MALDI-MS) spectra were obtained on a MALDI-time of flight/time of flight (TOF/TOF) instrument (UltrafleXtreme, Bruker Daltonics, Bremen, Germany) equipped with a 1-kHz smartbeam II laser (Nd: YAG–355 nm). The spectra were acquired in the negative and positive reflector ion modes in the mass range (m/z) between 100 and 1700. Nitric oxide was determined by chemiluminescence following a published procedure. Sample aliquots of aqueous **(I)** and **(II)** were injected into a vessel under argon atmosphere in the presence of VCl_3 (80 °C) and 1 M HCl (95 °C). The resulting NO reacted with O_3 in the detector. The chemiluminescent reaction was quantified and integrated with a photomultiplier tube/computer system.

The fluorescence lifetime of the compounds was determined on an Olympus MT 200–PicoQuant confocal microscope coupled to a laser with 470-nm excitation wavelength and filter BLP01-488R. Samples were dissolved in water, and data extracted from the decay curve were processed and fitted to an exponential decay curve by using the software OriginLab® 8.

Nitric oxide delivery was studied by employing the Nitric Oxide Analyzer Sievers 280i (General Electric) and the software Liquid Program. Samples were analyzed as follows: a 45 mM ascorbic acid solution was used as reducer, and samples containing ruthenium complexes at known concentration were added to the solution. The delivered NO was recorded on a Nitric Oxide Analyzer device in mV as a function of time. Integration of each peak gave the amount of delivered NO in mols. For quantification, a calibration curve with $NaNO_2$ solutions at different concentrations was used.

2.4. Cell culture conditions and cytotoxic assay

The B16F10 murine melanoma and human melanoma (C8161) cell lines were originally obtained from the American Type Culture Collection (Rockville, MD). The cell lines were allowed to grow to confluence in RPMI 1640 medium with phenol red and supplemented with 10% FCS, glutamine, and antibiotics at 37 °C, in 5% CO_2 and 95% air humidified atmosphere. All the reagents were purchased from Gibco-Invitrogen, Carlsbad, CA. The adherent cells were washed with PBS three times, sub-cultured by dispersion with trypsin–EDTA (2.5 g/L) (Sigma-Aldrich, St. Louis, Mo, USA), centrifuged at 1000 rpm and 10 °C for 15 min in complete medium, and seeded. The cells were placed in 96-well plates containing 0.2 mL of culture medium per well at a density of 5×10^4 cells per well. After 24 h of culture, the medium was removed, and fresh RPMI with different concentrations of each formulation of the tested compounds (2–150 μM) was added to the wells (stock solutions of the tested compounds (5 mg/mL) were prepared in dimethylsulfoxide (py-bodipy) and PBS (ruthenium complexes), and dilutions were performed in RPMI). The cells were incubated, and the solutions of the tested compounds were removed before the fresh complete medium was added.

Cell viability was measured by determining mitochondrial activity with the 3-(4,5-dimethylthiazol-2-yl)diphenyltetrazolium bromide (MTT) assay, according to the method described by Mosmann [46]. To this end, the culture medium was replaced, 100 μL of MTT (0.5 mg/mL) was added to each well, and the cells were incubated at 37 °C for further 4 h. Subsequently, the resulting formazan crystals were dissolved in dimethylsulfoxide (200 μL/well) for 3 h. The absorbance of each well was measured at 570 nm on a μQuant ELISA microplate reader (BioTek Instruments, Winooski, VT). Cell viability is expressed as the percentage of these values in the treated cells as compared with non-treated (control) cells. Results are given as the arithmetic mean ± standard deviation (X ± S.D.) of six independent experiments. Cisplatin (50 μM) was used as a positive control. Statistical comparisons were made (Student's t-test with $P < 0.05$ as the minimal level of significance and one-way ANOVA) with the Prism 5.0 Version Software.

2.5. Cellular uptake experiments by flow cytometry

Cellular uptake of the tested compounds by the B16F10 cells was determined by using a fluorescence-activated cell scanner (BD FACSCanto, Becton Dickinson) equipped with an argon ion laser providing excitation at 488 nm. The cells were incubated with the tested compound (10 μM) for 1 h–24 h, washed, and re-suspended in PBS. The cell suspensions were excited, and the fluorescence signal corresponding to drug uptake was detected by using a 670-nm long-pass filter. Analyses were performed with the aid of the FACSDiva software. Each analyzed sample contained a minimum of 10^4 cells. Propidium iodide (Sigma) and trypan blue (Gibco) were used to mark viable cells.

2.6. Cellular uptake and intracellular localization by fluorescent imaging microscopy

The experiments were carried out with a Nikon Eclipse T*i* microscope. Specific staining probes were employed for the organelles. The mitochondria were stained with Rhodamine 123 (Sigma Chemical Co.). 4′,6-Diamino-2-phenylindole (DAPI) (Molecular Probe) was used to probe the nuclei. Filter sets L5 (BP 480 nm, FT505 nm, LP 527 nm) and A (BP 340–380 nm, FT 400 nm, LP 425 nm) were applied for Rhodamine 123 and DAPI, respectively. For all the fluorescence imaging experiments, the cells were grown in 96-well culture plates and washed after incubation and prior to measurements.

The intracellular concentrations of complexes **(I)** and **(II)** after 24 h incubation was analyzed by UV-visible spectrum and the data were converted to percentage uptake from the total added of **(I)** and **(II)**.

2.7. Statistical analysis

All the results are expressed as the mean ± standard error mean. Statistical analyses were accomplished using Two-way ANOVA and Bonferroni's correction to evaluate the interaction of factors; statistical significance was obtained by One-Way ANOVA and Newman-Keuls post-hoc test ($p < 0.05$).

3. Results and discussion

3.1. Synthesis and characterization of nitrogen oxide derivative ruthenium complexes

The synthesis of **(I)** was performed according to a conventional procedure [39,40] involving reduction of the nitrosyl ruthenium complex *cis*-$[Ru(NO_2)(dcbpy)_2(NO)]^{2+}$ followed by addition of the pyridine derivative ligand py-bodipy, to afford **(I)**. Elemental analysis fitted in with the proposed formula. The **(I)** MALDI-TOF spectrum acquired in the positive ion mode displayed a peak at m/z 961.15 (Supplementary material: Fig. S1), which resembled the value calculated for *cis*-$[Ru(py\text{-}bodipy)(dcbpy)_2(NO_2)]^+$ (m/z = 961.15). The aminopropyl-β-lactose moiety, obtained as described on Scheme 1, interacted with **(I)** via an amide bond. The product of the reaction between aminopropyl-β-lactose and **(I)** was characterized by ^1H NMR spectrum. Compared to the aminopropyl-β-lactose ^1H NMR spectrum (data provided in the Experimental section and Supplementary Material: Fig. S2), the **(II)** ^1H NMR spectrum presented chemical shifts between 3.81 and 3.13 ppm, assigned to β-lactose organic protons [47,48]. Even though peaks in the aromatic region were too weak to assign (possibly because of a deshielding effect due to the presence of ruthenium), comparison between the ^1H RMN spectra of the ligand and the two ruthenium py-bodipy complexes (Supplementary Material: Fig. S2) attested that aminopropyl-β-lactose bound to the ruthenium complex, as expected. The MALDI process for **(II)** results in fragmentation after the ions have exited the source, with highest molecular fragment containing ruthenium with m/z = 1511. Together with the ^1H RMN spectrum, the MALDI results confirmed that *cis*-$[Ru(py\text{-}bodipy)(dcbpy\text{-}aminopropyl\text{-}\beta\text{-}lactose)_2(NO_2)]^+$ had the chemical structure suggested in Fig. 1.

HPLC analysis of the compounds and comparison of their retention times (single injection of a mixture of both compounds) in different analyses confirmed that the synthesized species were pure. The complexes had different retention times: **(I)** appeared as a single sharp peak at 2.0 min, whereas **(II)** eluted at 2.3 min (Supplementary Material: Figs. S3 and S4). As far as HPLC results are concerned, the ruthenium-nitrite complexes prepared herein were in high purity grade. On the basis of mass spectrometry, HPLC, and ^1HNMR analyses, we can infer that *cis*-$[Ru(py\text{-}bodipy)(dcbpy\text{-}aminopropyl\text{-}\beta\text{-}lactose)_2(NO_2)]^+$ (Fig. 1) originated from a coupling reaction between the lactose derivative compound and **(I)**.

Table 1 lists the electronic spectral data of the compounds synthesized here.

The ligand py-bodipy absorption spectrum resembled the absorption spectrum previously reported for bodipy derivatives [13,39]. The py-bodipy UV/Vis spectrum displayed a sharp absorption peak around 500 nm, attributed to the S0-S1 transition, and a shoulder around 475 nm, which was typical of a dipyrromethene framework vibronic sequence and referred to the S0-S2 transition [39]. The spectrum of *cis*-

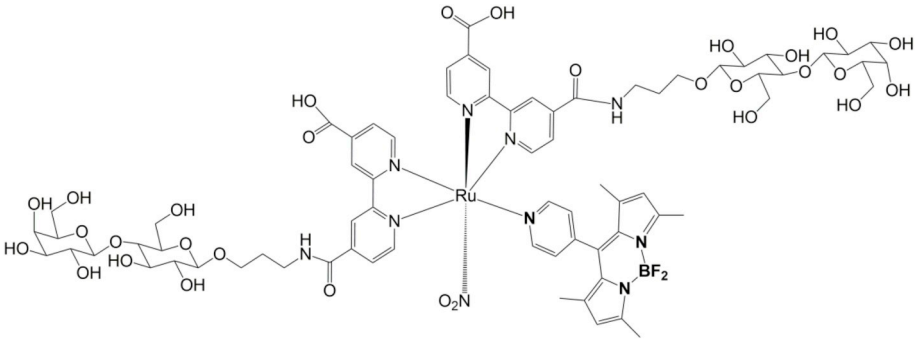

Fig. 1. Proposed chemical structure of *cis*-[Ru(py-bodipy)(dcbpy-aminopropyl-β-lactose)$_2$(NO$_2$)]$^{2+}$, based on ^{1}H NMR and MALDI analysis.

Table 1
Electronic spectral data and ν(NO) frequencies for the ligand py-bodipy and the ruthenium-nitrite complexes.

Compound	λ (nm) log ε	ν(NO) (cm^{-1})
py-bodipy	502 (5.83)[a], 475 (sh)	-
A	305 (4.0), 333 (3.92)[b]	1940
(I)	305 (4.6), 364 (4.1), 500 (4.13)[b]	-
(II)	305, 364, 500[b]	-

A = *cis*-[Ru(dcbpy)$_2$(NO)(NO$_2$)](PF$_6$)$_2$; **(I)** = *cis*-[Ru(py-bodipy)(dcbpy)$_2$(NO$_2$)](PF$_6$).
(II) = *cis*-[Ru(py-bodipy)(dcbpy-aminopropyl-β-lactose)$_2$(NO$_2$)](PF$_6$).
[a] Date collected in ethanol.
[b] Data collected in water.

Table 2
Parameters of the emission spectra, fluorescence lifetime, and quantum yields for **(I)** and its aminopropyl-β-lactose derivative.

Compound	λ_{em}	ϕ	$\tau_{1\ (\nu\sigma)}$	$\tau_{2\ (\nu\sigma)}$
py-bodipy	525	0.230[a]	0.4	-
(I)	515	0.019[b]	0.49	1.95
(II)	515	0.016[b]	5.43	1.49

(I) = *cis*-[Ru(py-bodipy)(dcbpy)$_2$(NO$_2$)](PF$_6$); **(II)** = *cis*-[Ru(py-bodipy)(dcbpy-aminopropyl-β-lactose)$_2$(NO$_2$)](PF$_6$).
λ_{exc} = 500 nm.
[a] Spectra recorded in ethanol.
[b] Spectra recorded in water.

[Ru(dcbpy)$_2$(NO)(NO$_2$)](PF$_6$)$_2$ differ of its precursor *cis*-[RuCl$_2$(dcbpy)$_2$] [43] mainly due the nitrogen oxide derivative ligand effect on the dπ-orbital energy. The band at 520 nm observed on *cis*-[RuCl$_2$(dcbpy)$_2$], characterized as a metal ligand charge transfer transition (MLCT) involving d$_\pi$ Ru(II) - π* (dcbpy) orbitals, disappeared. Such spectroscopic change was due to d$_\pi$ Ru(II) - π* (NO$^+$) back-bonding, which stabilized the dπ ruthenium orbitals and shifted this MLCT band to the ultraviolet region. Essentially, bands in UV region between nitrogen oxide derivative ruthenium complexes and its precursor remain similar, which bands are attributed to π - π* centered on the unsaturated ligand. Finally, in the case of **(I)** (Table 2, entry III), the band at 364 nm corresponded to MLCT involving d$_\pi$ Ru(II) → π* (dcbpy) orbitals, whilst the absorption band at 500 nm region resulted from the lowest-energy spin-allowed π-π* transitions involving the py-bodipy moiety. The coupling reaction between **(I)** and aminopropyl-β-lactose, which gave **(II)**, did not change the absorption bands, suggesting that this coupling did not modify the **(I)** spectroscopic features. The FTIR assignments of the complex **(I)** and its aminopropyl-β-lactose derivative revealed mainly intense peaks between 1000 and 1400 cm^{-1}, attributed to F-B bond stretching vibration in the py-bodipy moiety (data not shown). We assigned the intense peak at 1600 cm^{-1} to the C=N–B bond [48]. In addition, the **(II)** FTIR spectrum showed two bands, at 3342 and 2900 cm^{-1}, ascribed to $\nu_{N\text{-}H}$ stretching. Only *cis*-[Ru(dcbpy)$_2$(NO)(NO$_2$)](PF$_6$)$_2$ complex (Table 2) presented ν_{NO} stretching, attributed by comparison to similar species [49–51].

The intense py-bodipy fluorescence prompted us to study the photophysical properties of the ruthenium-nitrite complexes. The method described by Eaton [52] and based on Equation (1) (Experimental section) helped us to determine the fluorescence quantum yields of the synthesized complexes. We have used [Ru(bipy)$_3$]Cl$_2$ as standard because it displays absorption and emission bands near the bands of the studied complexes, which allowed it to be excited at the same wavelength. Table 2 summarizes the photophysical parameters of the ligand py-bodipy and the ruthenium complexes containing py-bodipy as ligand. The emission spectra of **(I)** and its aminopropyl lactose derivative were identical: both emitted at 515 nm, indicating that lactose functionalization did not disturb the **(I)** electronic structure.

The ruthenium complexes had lower quantum yield than the ligand py-bodipy, which indicated that py-bodipy moiety insertion resulted in higher energy dissipation via non-radiative pathways, thereby decreasing the fluorescence quantum yield and the fluorescence lifetime. The **(I)** functionalization with aminopropyl-β-lactose did not alter the photophysical properties significantly. We also measured luminescence lifetime for both ruthenium-(py-bodipy) derivative species. The time-resolved luminescence decay curves of the ruthenium complexes revealed best fitting supported as bi-exponential, while it was found the mono-exponential decay model for free py-bodipy (Table 2). For all the fluorescent species, the abundance of the first and the second component were about 55 and 45%, respectively. We attributed the second component to the ruthenium moiety, which could present some molecular orbital coupling with the py-bodipy ligand, leading to efficient quenching by energy transfer process.

3.2. Internalization of the complexes in cells

Two different techniques helped to determine the cellular uptake: flow cytometry and fluorescence image microscopy. Both methods are based on cell fluorescence intensity, which is enhanced by the luminescent ruthenium-nitrite complexes. This study aimed to elucidate how the molecular structure of the ruthenium-nitrite complexes influenced drug penetration, intracellular distribution, and subcellular localization and to correlate this information with the cytotoxicity and chemical structure of the investigated complexes. Furthermore, comparison of imaging and therapeutic functions could be interesting to develop a more specific, personalized medicine in a novel process known as theranostics [53,54].

Fluorescence imaging microscopy helped us to examine internalization of the target complexes by B16F10 cells. We incubated the cells with 10 μM of **(I)** or **(II)** for different periods (30 min–4 h). Fig. 2 depicts images of the studied bodipy derivative compounds (BDCs) in the cells. In cellular medium, fluorescence emission varies as a function of the incubation time. According to Fig. 2, the cells internalized the ruthenium complexes after 30 min of incubation. The cell images showed multiple fluorescent dots at the cell membrane surface. After incubation for 1 h, the complexes inside the cytoplasm had diffuse fluorescence, and the cells presented intense fluorescence, which revealed that the complexes were fully internalized. Images did not vary

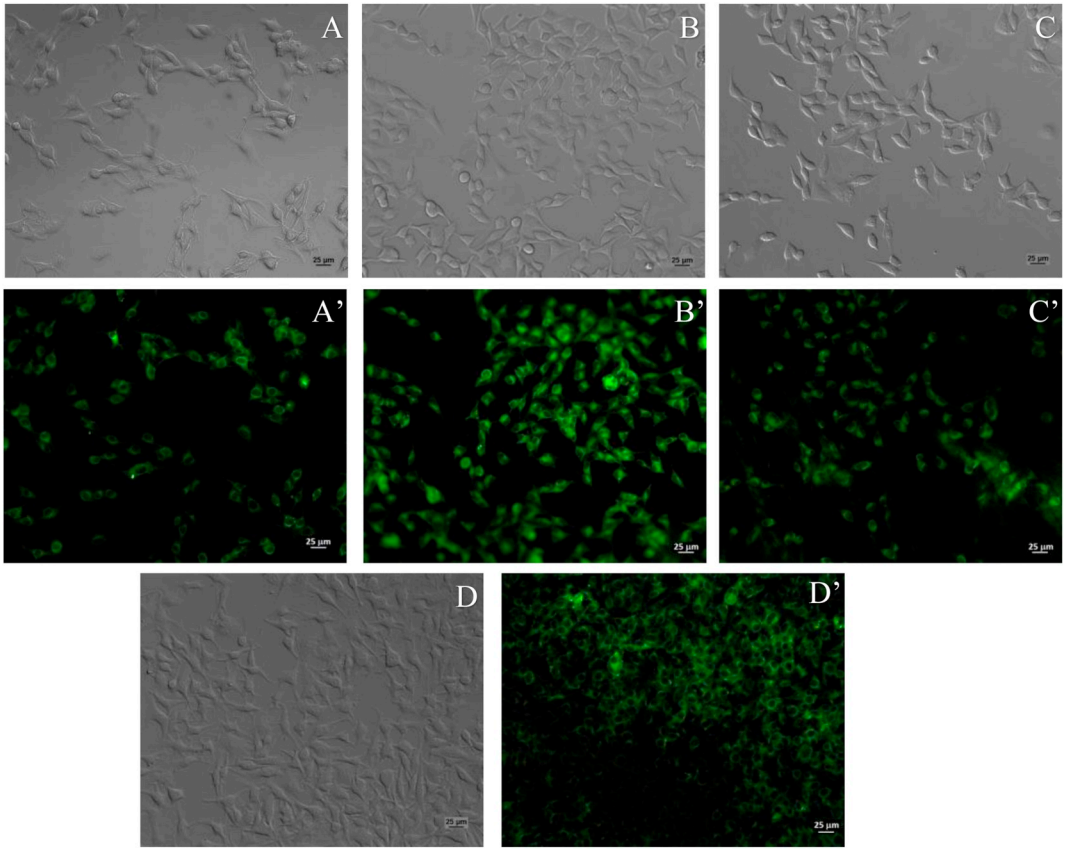

Fig. 2. Fluorescence microscopy images of B16F10 cells after incubation with (A′) **(I)** (10 µM) for 30 min, (B′) **(I)** (10 µM) for 1 h, (C′) **(I)** (10 µM) for 4 h, and (D′) **(II)** (10 µM) for 1 h. Bright field images of **(I)** (10 µM) corresponding to all the incubation time. (bar = 25 µm).

between 1 h and 4 h of incubation. However, more efficiently cellular uptake could be observed for **(II)** after 1 h incubation time. It seems therefore that the internalization of the BDCs is facilitated by the aminopropyl lactose moiety.

The monitoring of the intracellular spatial distribution of the compound **(II)** shows that it rapidly crosses the membrane in B16F10 cells, which coupled with NO release are involved in cellular cytotoxicity of ruthenium complexes. The Fig. 3 shows the cross-sectional diffusion of **(II)** (pixel intensity) after 1 h incubation time.

As a preliminary study of subcellular localization, we compared the fluorescence emission pattern of the investigated ruthenium compounds with the emission characteristics of standard probes (Rhodamine 123, a probe for mitochondria [55], and DAPI, a probe for nuclei [56]), aiming to identify the intracellular location of the target complexes (Fig. 4). Those probes could provide some evidence for the subcellular localization of **(I)** and **(II)** complexes. On the basis of the comparison between the BDC and DAPI fluorescence patterns, it seemed unlikely that **(I)** and **(II)** localized in the nucleus. Nevertheless, the BDCs shared similar fluorescence patterns with Rhodamine-123—the fluorescence bands overlapped, suggesting that the ruthenium complexes preferentially localized in regions near mitochondria. This organelle plays a significant role in cell metabolism, which emphasizes the importance of subcellular target in chemotherapy process. NO inhibits mitochondrial respiration, leading to cell death by apoptosis [15,57].

Flow cytometry analysis also helped to evaluate cellular uptake. Fluorescence-gated cells revealed whether the ruthenium-nitrite

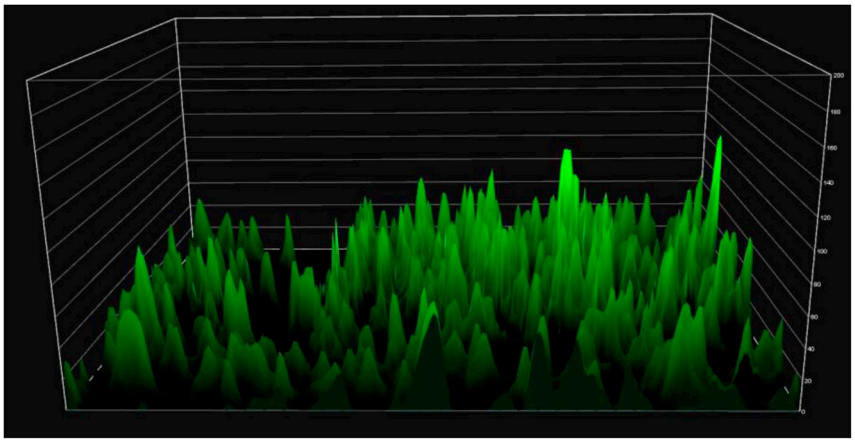

Fig. 3. Intensity surface plot of **(II)** after 1 h incubation time in B16F10 cells.

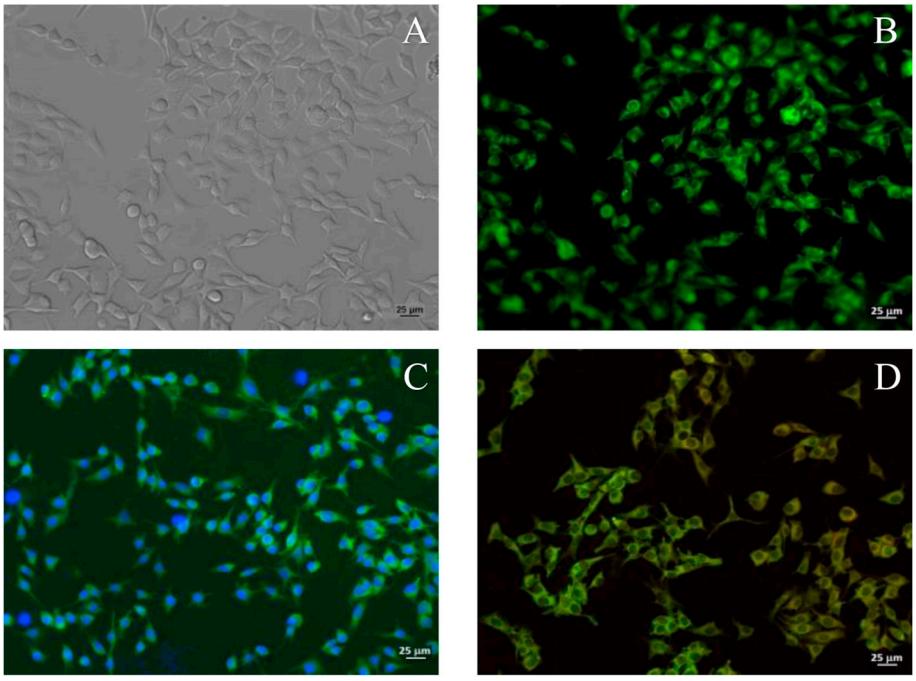

Fig. 4. Fluorescence microscopy images of B16F10 cells after incubation with (A) Bright field images of **(I)** (10 µM) after 1 h incubation, (B) **(I)** (10 µM) for 1 h, (C) Superposition of **(I)** (10 µM) and DAPI after 1 h incubation time, (D) Superposition of **(I)** (10 µM) and Rhodamine 123 after 1 h incubation time. (bar = 25 µm).

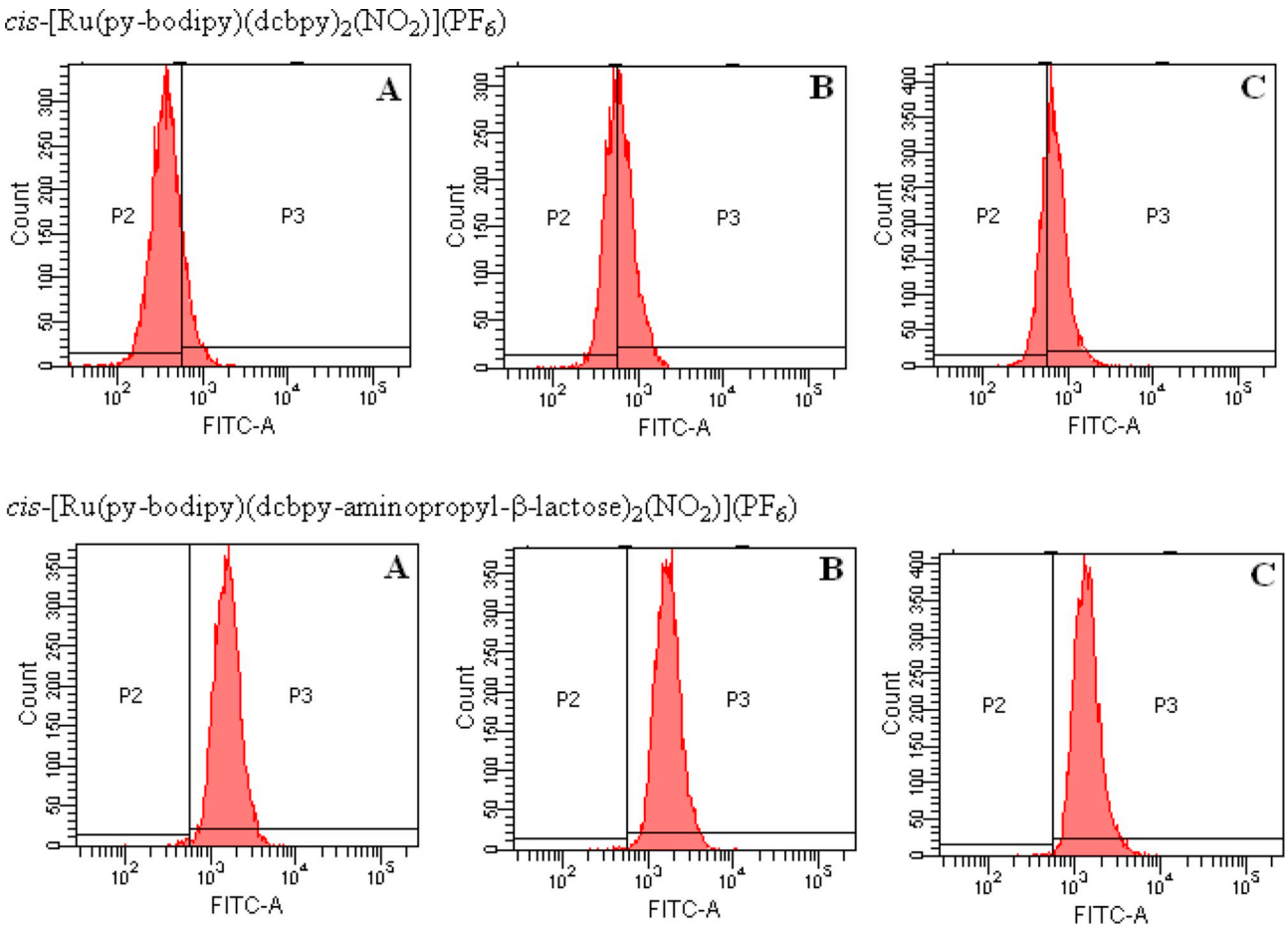

Fig. 5. Fluorescence histograms of cells with 10 µM of **(I)** and **(II)** after (A) 1 h; (B) 3 h and (C) 12 h. Cellular uptake was measured on channel P3, as exposed in the figure.

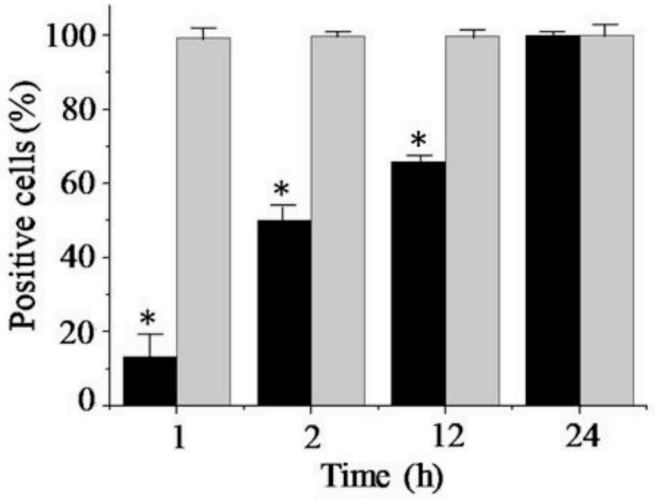

Fig. 6. Cellular uptake of ruthenium-nitrite complexes (10 μM) (black bars) **(I)** and (gray bars) **(II)**, in B16F10 cells, obtained by flow cytometry. (*: p value < 0.05). All *in vitro* experiments were performed in triplicate and expressed ad the mean ± standard deviation.

complexes were internalized. Flow cytometry analysis provided the cellular distribution of the complexes by means of filters that separated the emission wavelength of the compounds, affording a statistical percentage of the cells that internalized the complexes. Here, we incubated the B16F10 cells with **(I)** or **(II)** at 10 μM for different periods to evaluate whether functionalization with aminopropyl-β-lactose made the complex enter the cell more easily. It may happen via binding to lectins on cancer cells through glycosylation as described for species with similar structure moieties [58].

Fig. 5 shows the flow cytometry internalization measurement after incubation for 1–12 h.

Fig. 6 demonstrates how ruthenium-nitrite complex internalization depended on time as assessed by flow cytometry. After incubation for 60 min, only 13% of the cells internalized the complex **(I)**; the maximum cellular uptake was reached only after 24 h of incubation. B16F10 cells rapidly took up **(II)**, reaching 99% cellular uptake after incubation for 60 min (Fig. 5). Rapid **(II)** uptake by the cells suggested that the presence of the aminopropyl-β-lactose moiety favored their internalization in the cell, probably via specific binding to lectins through glycosylation of this moiety.

3.3. Cytotoxicity assays

The isolated **(I)** and **(II)** compounds were evaluated for cytotoxicity against B16F10 cells. According NO release analysis under reductive environment in a NO analyzer, both **(I)** and **(II)** are NO producer agents (Fig. 7). Similar process could be expected to happen after cellular uptake of ruthenium complexes, which NO release has been associated with a reduction process or oxygen transfer reaction for similar species [22–25].

Comparison curves of NO measurements using NO-sensor between **(I)** and **(II)** over a broad concentration range in B16F10 cancer cells in culture (10–200 μM) were recorded. Based on NO measurement as a function of time we have found that 150 μM of ruthenium complexes reached maximum NO concentration release after 24 h. Using that concentration cell viability was reached by MTT assays and show that both compounds caused ca. 75% of cell death (Fig. 8). The cytotoxicity was attributed to NO release as it appears to be inhibitory on cancer depending on its concentration [59–61].

The efficiencies of cellular uptake of compound **(I)** and **(II)** measured by UV-visible spectrum were found as 3.6 and 6.2% respectively. This finding well corroborated with our cell viability studies, with

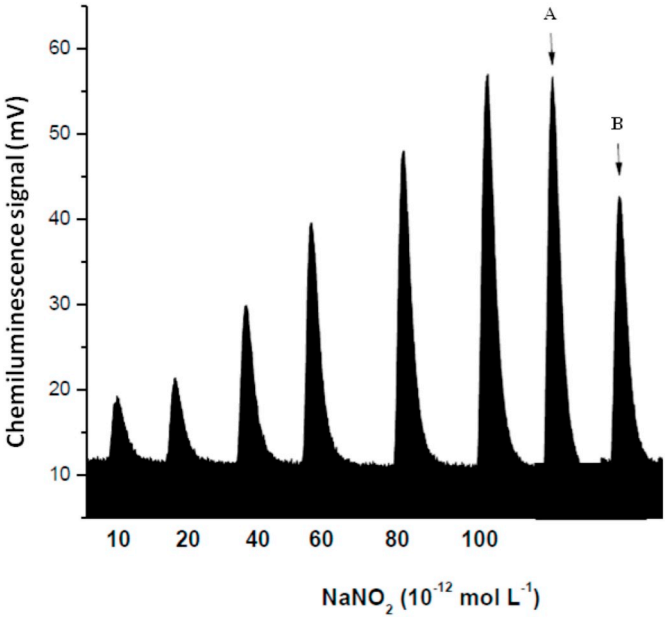

Fig. 7. NO release from an aqueous solution of sodium-nitrite. (A) Chemiluminescence NO detection of aqueous 1×10^{-10} M **(I)**; (B) NO detection of aqueous 1×10^{-10} M **(II)**.

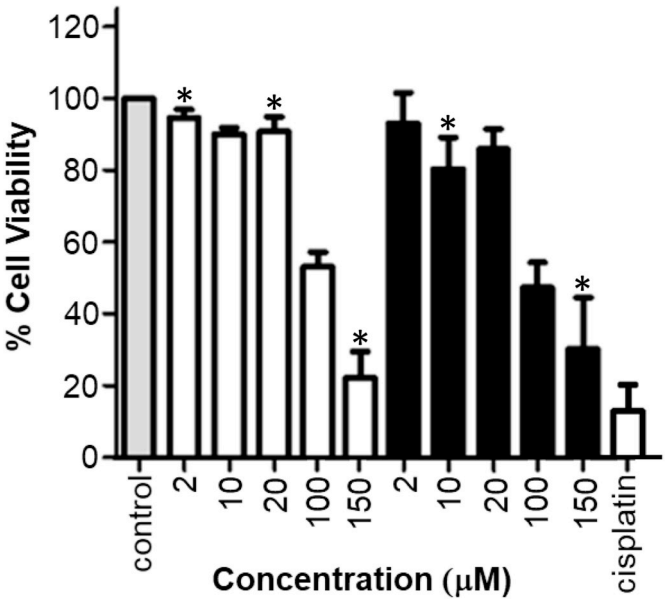

Fig. 8. B16F10 cancer cells exhibit concentration-dependent decrease for **(I)** (white) and **(II)** (black) after 24 h incubation. Cisplatin (50 μM) was used as a positive control. (*: p value < 0.05). All *in vitro* experiments were performed in hexplicate and expressed ad the mean ± standard deviation.

appreciable cytotoxicity only with 150 μM was used as maximum concentration of ruthenium complexes.

Because cell viability decreased with rising BDC concentration, our data suggest that NO production was primarily responsible for the mechanism that sensitized B16F10 cells. Our findings confirmed that the cytotoxic effect depended on NO concentration and was activated in a reductive cell environment. Cytotoxic assays using low BDC concentration led to cell growth, whereas higher BDC concentrations reduce cell viability. Those results corroborated with data from earlier studies demonstrating the dichotomous NO nature [62–64]. NO released from ruthenium-nitrite complexes may be involved in cell growth or inhibition, depending on their concentration.

4. Conclusions

Ruthenium-nitrite complexes are mainly internalized in mitochondria. These organelles are the major intracellular sources and targets of reactive species and have been associated with both cell necrosis and apoptosis. The aminopropyl lactose moiety enhances cellular uptake of the complex as a function of time probably via specific binding to lectins through glycosylation. The fluorescent complexes **(I)** and **(II)** exert considerable beneficial effects in terms of reduced B16F10 cell viability depending on the ruthenium complex concentration. Judging from these results, further investigation into these constructs could be very promising for future studies of *in vivo* chemo-sensitivity tests.

Acknowledgments

We thank Fundação de Amparo à Pesquisa do Estado de São Paulo (FAPESP) (2016/12707-0), CNPq, and CAPES for financial support.

Appendix A. Supplementary data

Supplementary data to this article can be found online at https://doi.org/10.1016/j.niox.2019.02.005.

References

[1] C.S. Allardyce, P.J. Dyson, Ruthenium in medicine: current clinical uses and future prospects, Platin. Met. Rev. 45 (2) (2001) 62–69.
[2] K.L. Haas, K.J. Franz, Application of metal coordination chemistry to explore and manipulate cell biology, Chem. Rev. 109 (10) (2009) 4921–4960.
[3] S.H. Van Rijt, P.J. Sadler, Current applications and future potential for bioinorganic chemistry in the development of anticancer drugs, Drug Discov. Today 14 (23) (2009) 1089–1097.
[4] N. Graf, S.J. Lippard, Redox activation of metal-based prodrugs as a strategy for drug delivery, Adv. Drug Deliv. Rev. 64 (11) (2012) 993–1004.
[5] L. Kelland, The resurgence of platinum-based cancer chemotherapy, Nat. Rev. Canc. 7 (8) (2007) 573–584.
[6] Z.H. Siddik, Cisplatin: mode of cytotoxic action and molecular basis of resistance, Oncogene 22 (47) (2003) 7265–7279.
[7] C.A. Rabik, M.E. Dolan, Molecular mechanisms of resistance and toxicity associated with platinating agents, Cancer Treat Rev. 33 (1) (2007) 9–23.
[8] M.A. Fuertes, C. Alonso, J.M. Pérez, Biochemical modulation of cisplatin mechanisms of action: enhancement of antitumor activity and circumvention of drug resistance, Chem. Rev. 103 (3) (2003) 645–662.
[9] C.W. Schwietert, J.P. McCue, Coordination compounds in medicinal chemistry, Coord. Chem. Rev. 184 (1) (1999) 67–89.
[10] N. Farrell, Transition Metal Complexes as Drugs and Chemotherapeutic Agents vol. 11, Springer Science & Business Media, 2012.
[11] P.C. Bruijnincx, P.J. Sadler, New trends for metal complexes with anticancer activity, Curr. Opin. Chem. Biol. 12 (2) (2008) 197–206.
[12] S. Banfi, E. Caruso, E. Zaza, M. Mancini, M. Gariboldi, E. Monti, Synthesis and photodynamic activity of a panel of BODIPY dyes, J. Photochem. Photobiol., A 114 (2012) 52–60.
[13] P. Farrás, A.C. Benniston, Bodipy-ruthenium(II) tris-bipyridyl dyads for homogeneous photochemical oxidations, Tetrahedron Lett. 55 (2014) 7011–7014.
[14] S.H. Lim, C. Thivierge, P. Nowak-Sliwinska, J. Han, H. van den Bergh, G. Wagnières, K. Burgess, H.B. Lee, In vitro and in vivo photocytotoxicity of boron dipyrromethene derivatives for photodynamic therapy, J. Med. Chem. 53 (2010) 2865–2874.
[15] D.A. Wink, J.B. Mitchell, Chemical biology of nitric oxide: insights into regulatory, cytotoxic, and cytoprotective mechanisms of nitric oxide, Free Radic. Biol. Med. 25 (1998) 434–456.
[16] A.G. Tennyson, S.J. Lippard, Generation, translocation, and action of nitric oxide in living systems, Chem. Biol. 18 (10) (2011) 1211–1220.
[17] E. Tfouni, D.R. Truzzi, A. Tavares, A.J. Gomes, L.E. Figueiredo, D.W. Franco, Biological activity of ruthenium nitrosyl complexes, Nitric Oxide 26 (2012) 38–53.
[18] S.K. Choudary, M. Chaudhary, S. Bagde, A.R. Gadbail, V. Joshi, Nitric oxide and cancer: a review, World J. Surg. Oncol. 11 (2013) 118.
[19] F.S. Oliveira, K.Q. Ferreira, D. Bonaventura, L.M. Bendhack, A.C. Tedesco, S.D.P. Machado, E. Tfouni, R.S. da Silva, The macrocyclic effect and vasodilation response based on the photoinduced nitric oxide release from trans-[RuCl(tetraazamacrocycle)NO]$^{2+}$, J. Inorg. Biochem. 101 (2) (2007) 313–320.
[20] N.L. Fry, P.K. Mascharak, Photoactive ruthenium nitrosyls as NO donors: how to sensitize them toward visible light, Acc. Chem. Res. 44 (4) (2011) 289–298.
[21] S.A. CicillinI, A.C.L. Prazias, A.C. Tedesco, O.A. Serra, R.S. Silva, Nitric oxide and singlet oxygen photo-generation by light irradiation in the phototherapeutic window of a nitrosyl ruthenium conjugated with a phthalocyanine rare earth complex, Polyhedron 28 (2009) 2766–2770.
[22] F.R. Keene, D.J. Salmon, J.L. Walsh, H.D. Abruna, T.J. Meyer, Oxidation of the ligand in nitro complexes of ruthenium(III), Inorg. Chem. 19 (7) (1980) 1896–1903.
[23] D. Ooyama, H. Nagao, N. Nagao, F.S. Howell, M. Mukaida, Some mechanistic evidence for an oxygen transfer reaction accompanied by the redox-induced nitrito-nitro linkage isomerization of ruthenium complex having nitrosyl, cis-[Ru(NO)(X)(bpy)$_2$]$^{2+}$ (X = ONO, NO$_2$), Chem. Lett. 759 (9) (1996) 759–760.
[24] Z.N. Rocha, M.S.P. Marchesi, J.C. Molin, C.N. Lunardi, K.M. Miranda, L.M. Bendhack, P.C. Ford, R.S. da Silva, The inducing NO-vasodilation by chemical reduction of coordinated nitrite íon in cis-[Ru(NO$_2$)L(bpy)$_2$]$^+$ complex, Dalton Trans. 28 (2008) 4282–4287.
[25] F.P. Rodrigues, C.R. Pestana, A.C. Polizello, G.L. Pardo-Andreu, S.A. Uyemura, A.C. Santos, L.C. Alberici, R.S. da Silva, C. Curti, Release of NO from a nitrosyl ruthenium complex through oxidation of mitochondrial NADH and effects on mitochondria, Nitric Oxide 26 (3) (2012) 174–181.
[26] D. Bonaventura, R.G. de Lima, J.A. Vercesi, R.S. da Silva, L.M. Bendhack, Vasc. Pharmacol. 46 (3) (2007) 215–222.
[27] L.J. Ignarro, C. Napoli, J. Loscalzo, Nitric oxide donors and cardiovascular agents modulating the bioactivity of nitric oxide, Circ. Res. 90 (1) (2002) 21–28.
[28] D. Bonaventura, F.S. Oliveira, V. Togniolo, A.C. Tedesco, R. Da Silva, L.M. Bendhack, A macrocyclic nitrosyl ruthenium complex is a NO donor that induces rat aorta relaxation, Nitric Oxide 10 (2004) 83–91.
[29] J.J.N. Silva, P.M. Guedes, A. Zottis, T.L. Balliano, F.O. Nascimento Silva, L.G.F. Lopes, J. Ellena, G. Oliva, A.D. Andricopulo, D.W. Franco, J.S. Silva, Novel ruthenium complexes as potential drugs for Chagas's disease: enzyme inhibition and in vitro/in vivo trypanocidal activity, Br. J. Pharmacol. 160 (2) (2010) 260–269.
[30] P.M. Guedes, F.S. Oliveira, F.R. Gutierrez, G.K. da Silva, G.J. Rodrigues, L.M. Bendhack, D.W. Franco, M.A.V. Matta, D.S. Zamboni, R.S. da Silva, J.S. Silva, Nitric oxide donor trans-[RuCl([15]aneN$_4$)NO]$^{2+}$ as a possible therapeutic approach for Chagas' disease, Brit, J. Pharmacol. 160 (2) (2010) 270–282.
[31] T.A. Heinrich, A.C. Tedesco, J.M. Fukuto, R.S. da Silva, Production of reactive oxygen and nitrogen species by light irradiation of a nitrosyl phthalocyanine ruthenium complex as a strategy for cancer treatment, Dalton Trans. 43 (10) (2014) 4021–4025.
[32] L.C.B. Ramos, M.S.P. Marchesi, D. Callejon, M.D. Baruffi, C.N. Lunardi, L.D. Slep, L.M. Bendhack, R.S. da Silva, Enhanced antitumor activity against melanoma cancer cells by nitric oxide release and photosensitized generation of singlet oxygen from ruthenium complexes, Eur. J. Inorg. Chem. (2016) 3592–3597.
[33] V. Brabec, O. Nováková, DNA binding mode of ruthenium complexes and relationship to tumor cell toxicity, Drug Resist. Updates 9 (3) (2006) 111–122.
[34] E. Alessio, G. Mestroni, A. Bergamo, G. Sava, Ruthenium antimetastatic agents, Curr. Top. Med. Chem. 4 (15) (2004) 1525–1535.
[35] W. Xu, L.Z. Liu, M. Loizidou, M. Ahmed, I.G. Charles, The role of nitric oxide in cancer, Cell Res. 12 (5–6) (2002) 311–320.
[36] S. Burney, J.L. Caulfield, J.C. Niles, J.S. Wishnok, S.R. Tannenbaum, The chemistry of DNA damage from nitric oxide and peroxynitrite, Mutat. Res. 424 (1–2) (1999) 37–49.
[37] L. Ignarro, Nitric Oxide: Biology and Pathobiology, Academic Press, San Diego, 2000.
[38] A.R. Oki, R.J. Morgan, An efficient preparation of 4, 4′-dicarboxy-2, 2′-bipyridine, Synth. Commun. 25 (43) (1995) 4093–4097.
[39] L.C.D. Rezende, M.M. Vaidergorn, J.C.B. Moraes, F.S. Emery, Synthesis, photophysical properties and solvatochromism of meso-substituted tetramethyl BODIPY dyes, J. Fluoresc. 24 (1) (2014) 257–266.
[40] V.L. Campo, M.B. Martins, C.H.T.P. da Silva, I. Carvalho, Novel and facile solution-phase synthesis of 2,5-diketopiperazines and O-glycosylated analogs, Tetrahedron 65 (2009) 5343–5349.
[41] F.P. Dwyer, H.A. Goodwin, E.C. Gyarfas, Mono and bis(2,2'-bipyridine) and -(1,10-phenanthroline) chelates of ruthenium and osmium. II. Bischelates of bivalent and tervalent ruthenium, Aust. J. Chem. 16 (4) (1963) 544–548.
[42] J.B. Godwin, T.J. Meyer, Nitrosyl-nitrite interconversion in ruthenium complexes, Inorg. Chem. 10 (10) (1971) 2150–2153.
[43] M.G. Sauaia, R.S. da Silva, The reactivity of nitrosyl ruthenium complexes containing polypyridyl ligands, Trans. Met. Chem. 28 (2003) 254–259.
[44] A.T.R. Williams, S.A. Winfield, J.N. Miller, Relative fluorescence quantum yields using a computer-controlled luminescence spectrometer, Analyst 108 (1290) (1983) 1067–1071.
[45] U. Resch-Genger, P.C. DeRose, Fluorescence standards: classification, terminology, and recommendations on their selection, use, and production, Pure Appl. Chem. 82 (12) (2010) 2315–2335 2010.
[46] T. Mosmann, Rapid colorimetric assay for cellular growth and survival: application to proliferation and cytotoxicity assays, J. Immunol. Methods 65 (1–2) (1983) 55–63.
[47] Y. Wang, X. Huang, L.H. Zhang, X.S. Ye, A four-component one-pot synthesis of α-gal pentasaccharide, Org. Lett. 6 (24) (2004) 4415–4417.
[48] Y. Zhou, Z. Zhou, Y. Li, W. Yang, Synthesis and properties of BODIPY polymers and their photocatalytic performance for aerobic oxidation of benzylamine, Catal. Commun. 64 (2015) 96–100.
[49] M. Videla, J.S. Jacinto, R. Baggio, M.T. Garland, P. Singh, W. Kaim, L.D. Slep, J.A. Olabe, New ruthenium nitrosyl complexes with tris(1-pyrazolyl)methane (tpm) and 2,2‘-bipyridine (bpy) coligands. Structure, spectroscopy, and electrophilic and nucleophilic reactivities of bound nitrosyl, Inorg. Chem. 45 (21) (2006) 8608–8617.
[50] R.G. de Lima, M.G. Sauaia, D. Bonaventura, A.C. Tedesco, L.M. Bendhack, R.S. da Silva, Influence of ancillary ligand L in the nitric oxide photorelease by the [Ru(L)(tpy)NO]$^{3+}$ complex and its vasodilator activity based on visible light irradiation, Inorg. Chim. Acta 359 (8) (2006) 2543–2549.
[51] M.G. Sauaia, F.S. Oliveira, A.C. Tedesco, R.S. da Silva, Control of NO release by light irradiation from nitrosyl–ruthenium complexes containing polypyridyl

ligands, Inorg. Chim. Acta 355 (2003) 191–196.
[52] F. Eaton, Reference materials for fluorescence measurement, Pure Appl. Chem. 60 (7) (1988) 1107–1114.
[53] O. Mazuryk, M. Maciuszek, G. Stochel, F. Suzenet, M. Brindell, 2-Nitroimidazole-ruthenium polypyridyl complex as a new conjugate for cancer treatment and visualization, J. Inorg. Biochem. 134 (2014) 83–91.
[54] C.T. Poon, P.S. Chan, C. Man, F.L. Jiang, R.N. Wong, N.K. Mak, D.W. Kwong, S.W. Tsao, W.K. Wong, An amphiphilic ruthenium(II)-polypyridyl appended porphyrin as potential bifunctional two-photon tumor-imaging and photodynamic therapeutic agent, J. Inorg. Biochem. 104 (2010) 62–70.
[55] A. Baracca, G. Sgarbib, G. Solainib, G. Lenaza, Rhodamine 123 as a probe of mitochondrial membrane potential: evaluation of proton flux through F0 during ATP synthesis, Biochim. Biophys. Acta 1606 (2003) 137–146.
[56] J. Kapuscinski, DAPI: a DNA-specific fluorescent probe, Biotech. Histochem. 70 (5) (1995) 220–233.
[57] Z.A. Carneiro, J.C.B. Moraes, F.P. Rodrigues, R.G. Lima, C. Curti, Z.N. Rocha, M. Paulo, L.M. Bendhack, A.C. Tedesco, A.L.B. Formiga, R.S. da Silva, Photocytotoxic activity of a nitrosyl phthalocyanine ruthenium complex — a system capable of producing nitric oxide and singlet oxygen, J. Inorg. Biochem. 105 (2011) 1035–1043.
[58] Y. Hama, Y. Urano, Y. Koyama, P. Choyke, H. Kobayashi, Targeted optical imaging of cancer cells using lectin-binding BODIPY conjugated avidin, Biochem. Biophys. Res. Commun. 348 (2006) 807–813.
[59] P.K. Kim, R. Zamora, P. Petrosko, T.R. Billiar, The regulatory role of nitric oxide in apoptosis, Int. Immunopharmacol. 1 (8) (2001) 1421–1441.
[60] D. Fukumura, S. Kashiwagi, R.K. Jain, The role of nitric oxide in tumour progression, Nat. Rev. Canc. 6 (2006) 521–534.
[61] D.A. Wink, Y. Vodovotz, J. Laval, F. Laval, M.W. Dewhirst, J.B. Mitchell, The multifaceted roles of nitric oxide in cancer, Carcinogenesis 19 (5) (1998) 711–721.
[62] S.M. Janib, A.S. Moses, J.A. MacKay, Imaging and drug delivery using theranostic nanoparticles, Adv. Drug Deliv. Rev. 62 (11) (2010) 1052–1063.
[63] E.K. Lim, T. Kim, S. Paik, S. Haam, Y.M. Huh, K. Lee, Nanomaterials for theranostics: recent advances and future challenges, Chem. Rev. 115 (1) (2015) 327–394.
[64] R. Bardhan, S. Lal, A. Joshi, N.J. Halas, Theranostic nanoshells: from probe design to imaging and treatment of cancer, Acc. Chem. Res. 44 (10) (2011) 936–946.